Ab Initio Multiple Spawning Dynamics of Excited Butadiene: Role of Charge Transfer

Benjamin G. Levine[†] and Todd J. Martínez*[,‡]

Department of Chemistry and The Beckman Institute, University of Illinois, Urbana, Illinois 61801

Received: July 26, 2009; Revised Manuscript Received: September 4, 2009

Ab initio multiple spawning simulations of the photochemical reaction dynamics of *s-trans*-1,3-butadiene were performed. It is found that nonadiabatic events involving two low-lying excited states begin as early as 10 fs after excitation, resulting in the population being split between the bright 1^1B_u state and the dark 2^1A_g state. The molecule subsequently twists about a terminal carbon−carbon bond regardless of whether it is on the 1^1B_u or 2^1A_g electronic state. This twisting motion leads to conical intersections between S_1 and S_0. Several regions of the intersection seam involving states of differing character are accessed. The regions of the seam involving intersection between a state of charge-transfer character and a state of covalent character dominate the quenching dynamics, but intersections between two covalent states are also accessed a small percentage of the time. The existence and relative energies of these intersections are validated by optimization at the multistate complete active space second-order perturbation level of theory (MS-CASPT2). Our results point to a new mechanism for photoisomerization of butadiene that emphasizes the role of charge-transfer states.

Introduction

Cis−*trans* photoisomerization of conjugated organic molecules is an important class of photochemical reactions because these reactions convert light to mechanical energy on a molecular scale.[1,2] Photoinduced isomerization is the primary event in many photobiological processes including vision, ion pumping, and phototaxis.[2,3] Such biological systems demonstrate that this reaction can be harnessed to do useful work on the molecular scale, and it is likely that *cis*−*trans* photoisomerization will prove to be central in the development of rationally designed light-powered molecular machines.[2,4−6]

Despite its simple appearance, the photochemistry of butadiene, and of polyenes in general, is quite complicated, and over the years many possible mechanisms have been proposed. In this paper we apply first-principles quantum dynamical methods to elucidate the details of photochemical *cis*−*trans* isomerization in *trans*-1,3-butadiene. In contrast to previous theoretical investigations of the excited-state dynamics of butadiene,[7−9] we are able to *simultaneously* describe *both* of the low-lying valence excited states, vide infra. This leads to a significant revision of the currently accepted view of the excited-state reaction mechanism,[10,11] which is supported by potential energy surface optimizations using multireference methods that explicitly include dynamic electron correlation. The photochemistry of polyenes in general has been studied extensively both theoretically and experimentally. Thus, we begin with an overview of the key experimental and theoretical results to place our current work in the appropriate context. Throughout this paper, we focus on the linear *all-trans* polyenes unless explicitly stated otherwise.

Early studies of polyenes assumed that the lowest singlet excited state is the strongly allowed 1B transition that corresponds to a $\varphi_{HOMO} \rightarrow \varphi_{LUMO}$ excitation. However, significant evidence points to the involvement of a second (optically dark) low-lying valence state (referred to as 2A in the following). For example, the observed fluorescence lifetime in diphenyloctatetraene is considerably longer than the lifetime predicted by application of the Strickler−Berg equation,[12] suggesting the involvement of more than one excited electronic state.[13] Furthermore, the absorption spectrum depends strongly on solvent polarity, while the solvent dependence of the emission spectrum is so small that it is difficult to detect.[14] Hudson and Kohler succeeded in detecting a very weak absorption band at lower energy than the strongly absorbing 1B state in diphenyloctatetraene,[15,16] leading them to conclude that emission occurs after a fast radiationless transition from the 1B state to a lower lying dark 2A state in diphenyloctatetraene. Other polyenes exhibit similarly anomalous behavior. For example, the absorption and emission spectra in octatetraene lack mirror symmetry,[17−19] and there is an unusually large gap (∼0.5 eV) between the absorption and emission origins.[20−23] Therefore, Hudson and Kohler proposed that this scheme applies generally to the entire class of molecules.[15,16] Theoretical support for this proposal first came from Schulten and Karplus, who found that the doubly excited $\varphi^2_{HOMO} \rightarrow \varphi^2_{LUMO}$ configuration mixes with higher energy single excitations of A symmetry ($\varphi_{HOMO} \rightarrow \varphi_{LUMO+1}$ and $\varphi_{HOMO-1} \rightarrow \varphi_{LUMO}$) to stabilize the 2A state such that it is nearly degenerate with or even below the bright 1B state.[24]

It is now widely accepted that the 2A state plays an important role in the photochemistry of polyenes with four or more double bonds (henceforth referred to as the "longer polyenes".) However, the situation becomes less clear when the shortest linear polyenes, butadiene and hexatriene, are considered. Unlike longer polyenes, butadiene and hexatriene emit no detectable fluorescence,[25,26] and absorption to the 2A state of butadiene and hexatriene has not been detected. In addition, while the absorption spectra of *all-trans*-butadiene, -hexatriene, and -octatetraene in a supersonic jet exhibit very similar vibrational progressions, the widths of the absorption lines differ dramatically. The butadiene absorption spectrum has the broadest peaks, and the peaks get narrower as the conjugation length increases.[27,28] In fact, the spectroscopic features of the shorter polyenes more closely resemble ethylene than the longer

[†] Present address: Department of Chemistry, University of Pennsylvania, Philadelphia, PA.

[‡] Present address: Department of Chemistry, Stanford University, Stanford, CA.

10.1021/jp907111u CCC: $40.75
Published on Web 10/08/2009

polyenes. The $\pi \rightarrow \pi^*$ band of the absorption spectrum of ethylene is extremely broad,[29] and fluorescence has never been detected. Thus, it is possible that the photodynamics of butadiene and hexatriene may be more similar to those of ethylene than to those of the longer polyenes.

The photodynamics of ethylene are relatively well understood. In contrast to the longer polyenes, the 2A state in ethylene (generally referred to as the Z state) is much higher in energy than the 1B state (the V state). Thus, when ethylene is excited to the 1B state, the 2A state does not play a role in the dynamics until the molecule is significantly distorted. Instead of quickly transitioning to the 2A state while approximately planar, the molecule twists about the carbon−carbon bond. This twisting stabilizes the 2A state significantly and further allows mixing of the 1A, 1B, and 2A states because of the symmetry lowering. This mixing leads to a lowest adiabatic excited state with a large degree of intramolecular charge-transfer character. Unlike in the longer polyenes, the 2A state is not involved in the dynamics of ethylene until torsional distortion is so severe as to make the symmetry labels meaningless. Shortly after twisting, the ethylene molecule further undergoes elongation of a C−H bond and pyramidalization about one of the carbon atoms. These distortions stabilize the charge-transfer state and lead directly to a seam of conical intersections that mediate internal conversion to the ground state.[30−37] In competition with this dominant pathway, there is also the potential for the H atom in the elongated C−H bond to migrate across the C−C bond, forming ethylidene (CH_3CH). This H-migration pathway also leads to rapid electronic quenching through conical intersections.[30−37]

One possible explanation for the ethylene-like characteristics of butadiene and hexatriene is that the 2A state is higher in energy in these molecules than in the longer polyenes. As such the state ordering of the 2A and 1B states has been a subject of both theoretical[38−43] and experimental[44−53] inquiry. Although there remains some disagreement about the ordering of the 1B and 2A states at the Franck−Condon point in these molecules, these studies generally agree that (1) the gap between the states is small enough that they likely cross near the Franck−Condon region and (2) the 2A state lies below the 1B state after in-plane excited-state relaxation (which may or may not lead to a true minimum as discussed below). Both of these points support the conclusion that the 2A state can play a role in the dynamics of butadiene and hexatriene before out-of-plane distortion makes the 2A and 1B labels meaningless. (In practice the 2A and 1B states are clearly distinguishable until the molecule is more than 10° twisted.) This is in contrast to ethylene where the 2A (Z) state is only low enough in energy to play a role after significant (>45°) twisting about the carbon−carbon double bond.[32,54]

The energetic proximity of the 2A state does not guarantee that it is important to the initial dynamics, as it could be only weakly coupled to the 1B state in the Franck−Condon region (by symmetry there is no coupling for planar geometries, and coupling between these states is only possible by virtue of the finite width of the vibrational wave functions). Many researchers have studied whether butadiene and hexatriene transition to the 2A state before leaving the Franck−Condon region (i.e., while still effectively planar) like the longer polyenes or if they instead leave the Franck−Condon region on the 1B state by distortion along out-of-plane modes like ethylene. Resonance Raman results on both *cis*- and *trans*-hexatriene suggest that the frequencies associated with the double bond torsional mode are reduced but that there does exist a planar local minimum on the 1B state.[55−57] In contrast, the reduction of torsional frequencies in isoprene (2-methylbutadiene) is great enough to conclude

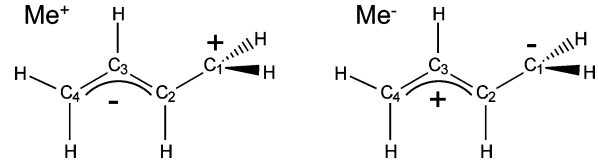

Figure 1. Allyl−methyl charge-transfer states in butadiene.

that there is no planar minimum on the 1B state in this molecule.[58] Time-resolved multiphoton ionization spectra find very short lifetimes (<100 fs) which are often assigned to a fast transition to the 2A state, but there is little evidence to exclude the possibility that these lifetimes instead correspond to fast out-of-plane distortion.[59,60]

Theoretical studies have found that the absorption spectra of the short polyenes can be well-described by reduced dimensionality models that exclude the out-of-plane modes.[61−68] This suggests that the initial dynamics is dominated by in-plane modes. However, these simulations always include an artificial broadening of the absorption spectrum and cannot provide an explanation for the large ($\sim$750 cm^{-1}) homogeneous broadening[28] of the butadiene absorption spectrum. Fast out-of-plane distortion could explain this broadening.

Thus, the short-time behavior of butadiene appears to be neither completely ethylene-like nor completely polyene-like. The first important question addressed in this paper centers on this short-time behavior. Is the initial step after excitation a fast electronic transition to the dark 2A state (as is the case in longer polyenes), or are electronic transitions preceded by a fast, large-amplitude geometric distortion, analogous to ethylene where the molecule twists significantly (more than 45°) around the double bond before any such electronic transition occurs? In fact, these two possibilities are not mutually exclusive. The population could bifurcate between the 1B and 2A states, and large-amplitude geometric distortions could proceed simultaneously on both states. Only a dynamical study that includes both excited states, such as the one presented in this paper, can address questions regarding the complex short-time dynamics of butadiene.

There is a second important question regarding butadiene photochemistry. The complete absence of fluorescence indicates a fast radiationless decay to the ground state, but the nature of this decay is not well understood. Experience with other photoisomerizing molecules suggests that one or more conical intersections are involved, but it remains to determine the photochemical mechanism, i.e., the pathways which dominate the dynamics. Proposals so far include intersections between covalent states (involving some degree of torsion about all three C−C bonds) and intersections involving charge-transfer states (often involving pyramidalization about one or more carbon atoms).

Early studies of butadiene generally suggested that nonadiabatic decay occurs via conical intersections involving charge-transfer states. A semiempirical study by Salem and Bruckman proposed the 3 × 3 configuration interaction (3 × 3-CI) model of butadiene,[69] which describes the three low-lying states of butadiene as linear combinations of three configurations: $|\psi_{core}\varphi^2_{HOMO}\rangle$, $|\psi_{core}\varphi_{HOMO}\varphi_{LUMO}\rangle$, and $|\psi_{core}\varphi^2_{LUMO}\rangle$. This model predicts that, after twisting about a double bond, butadiene can access two funnels on the excited state that lead to different photoproducts. These funnels correspond to oppositely charged zwitterionic states (pictured in Figure 1) which are stabilized by various distortions of the molecule, including pyramidalization of the negatively charged carbon. While the 3 × 3-CI model does include the important $|\psi_{core}\varphi^2_{LUMO}\rangle$ configuration, it does

not include either of the $\phi_{HOMO} \rightarrow \phi_{LUMO+1}$ and $\phi_{HOMO-1} \rightarrow \phi_{LUMO}$ singly excited configurations that contribute to the 2A state. Thus, it is not clear that this model is sufficiently flexible to describe the 2A state. Ohmine also suggested the possibility of surface crossing involving charge-transfer states in terminally twisted butadiene. These state crossings (either true or weakly avoided) are brought about by a hydrogen migration type motion,[70] which is analogous to similar findings in ethylene.[1]

The controversy regarding the involvement of charge-transfer states in butadiene photodynamics began when Aoyagi investigated the excited-state surfaces of butadiene using a complete active space self-consistent field (CASSCF) method including the four π electrons and four π orbitals in the active space.[71] These CAS(4/4) results painted a picture markedly different from that suggested by previous studies. Instead of a terminally twisted ionic S_1 minimum, the S_1 state is covalent (i.e., radicaloid) and its minimum is slightly twisted around both double bonds. Subsequent studies by Olivucci and co-workers, also using CAS(4/4), located several S_1/S_0 minimal energy conical intersections (MECIs) which are very close in energy and geometry to the S_1 minimum. These MECIs exhibit concerted rotation about multiple bonds and bear some resemblance to structures that would be expected in the "hula-twist" isomerization mechanism.[72] It is important to point out that the CAS(4/4) method is well-known to provide a poor description of the optically bright 1B state in *trans*-butadiene. In fact, CAS(4/4) predicts the 1B state to lie above the 2A state by approximately 2 eV, in contradiction to both experimental and high-level theoretical results (vide supra) which establish that the gap between these two excited states is very small.[39] Thus, conclusions from CAS(4/4) are only justified if the initially excited population on the 1B state decays very quickly to the covalent 2A state, before the molecule leaves the Franck−Condon region (i.e., while it is still effectively planar). Olivucci and co-workers assumed this to be the case, and the CAS(4/4) results then predict that this ultrafast 1B $\rightarrow$ 2A transition is followed by twisting on the 2A state and subsequent relaxation to the ground state via one of the radicaloid S_1/S_0 MECIs mentioned above. This radicaloid mechanism, where ionic and/or zwitterionic structures play no role, is the generally accepted mechanism of photoisomerization in butadiene today.[10,11,73]

Dynamical simulations have been carried out which support both the charge-transfer and radicaloid relaxation mechanisms. In both cases, the outcome is preordained by the electronic structure method used. Methods based on variants of density functional theory limited to singly excited states have been employed.[7,8] Since these methods cannot describe the 2A state correctly (they lack the necessary double excitations), they predict a relaxation mechanism analogous to that implied by the 3 × 3-CI model, with the ionic 1B state playing an important role. Dynamics calculations using semiempirical valence bond representations of the potential energy surfaces (PESs) have also been carried out.[9,74] In the form used, these semiempirical methods neglect ionic states, and thus, it is perhaps not surprising that they predict a radicaloid mechanism. Because they cannot describe ionic or zwitterionic states, all trajectories in these simulations begin on the 2A state, assuming an ultrafast radiationless transition from the 1B state.

As discussed above, neither the 3 × 3-CI nor the CAS(4/4) method can provide a satisfactory picture of the electronic structure in butadiene; the former treats the covalent states poorly (due to its lack of singly excited configurations which play an important role in the 2A state), while the latter treats the ionic states poorly (due to its lack of dynamic electron correlation effects). To understand the detailed photochemical mechanism for *trans*−*cis* isomerization in butadiene, one needs to use an electronic structure method which can treat both the 1B and 2A states in a balanced manner and thereby determine the potential interplay between dynamics on the two states. In this paper, we present the first such dynamical simulations of butadiene treating the ionic and covalent states in a balanced fashion. These simulations address both the short-time (does butadiene decay quickly to the dark state like a polyene or twist on the bright state like ethylene?) and long-time (does charge transfer play a role in the decay to the ground state?) dynamics of butadiene. The answers to these questions as presented in this paper are a departure from the currently accepted view of butadiene photochemistry, but are completely consistent with available experimental data. In support of our dynamical simulations, we present high-level static quantum chemical results to demonstrate the accuracy of the PESs employed in our dynamic simulation, to provide insight into the complex shape of these surfaces, and to point out possible biases in our dynamical data.

Theoretical Methods

All state-averaged CASSCF[75] and multistate complete active space second-order perturbation theory (CASPT2)[76,77] calculations are performed using the MOLPRO molecular electronic structure package without use of symmetry.[78−82] The use of the multistate CASPT2 (MS-CASPT2) method,[77] which allows the perturbed states to interact with each other, is critical when describing conical intersections because the perturbed states are degenerate. Geometry and conical intersection optimization at the MS-CASPT2 level of theory was performed using a penalty function method that does not require analytic gradients or nonadiabatic coupling vectors. This method has been previously described and implemented in our freely available CIOPT code.[83] Throughout this paper the active space employed in CASSCF and CASPT2 calculations will be abbreviated in the form SA*N*-CAS(*m*/*n*), where *N* is the number of singlet electronic states included in the state average (all states are equally weighted), *m* is the number of active electrons, and *n* is the number of active orbitals. The suffix -MSPT2 is appended to indicate MS-CASPT2.

Ab initio multiple spawning (AIMS) simulations[5,33,34,37,84] were carried out with an integrated code combining AIMS dynamics and the MOLPRO electronic structure package.[85] Twenty initial nuclear basis functions were run using the independent first-generation approximation.[85,86] The initial positions and momenta for these basis functions were sampled from the ground-state vibrational Wigner distribution in the harmonic approximation by a Monte Carlo procedure. The ground-state minimum geometry and frequencies used to obtain the Wigner distribution were calculated at the DFT level of theory using the BLYP functional and 6-31G basis set with the JAGUAR electronic structure package.[87] The initial basis functions were placed on the brighter of the two lowest singlet valence excited states to simulate excitation to the bright 1^1B_u state. By the end of the simulations, an average of 28 basis functions were spawned in each simulation; i.e., more than 550 trajectory basis functions are involved in the simulations described here. The electronic wave functions (and resulting PESs and nonadiabatic couplings) at each time step were calculated using an SA3-CAS(4/3) wave function and the 6-31G basis set. The equations of motion were integrated using a multiple time scale integration scheme[85] with a time step of 0.24 fs (10 au). The dynamics was followed for 200 fs after excitation.

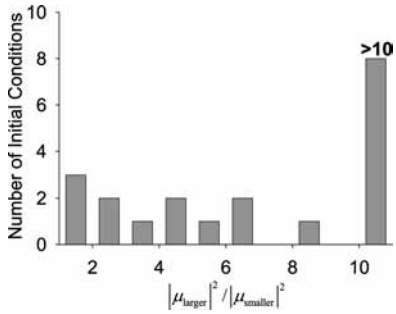

Figure 2. Histogram of the ratios of the squared transition dipole moments for the $S_0 \rightarrow S_1$ and $S_0 \rightarrow S_2$ transitions for the 20 initial nuclear basis functions. The ratios are calculated such that they are always greater than 1. In most cases the ratio is large, and thus, one of the adiabatic states can be unambiguously assigned as the bright 1^1B_u state. However, there are a few cases where the ratio is near 1. This indicates that the 1^1B_u and 2^1A_g states are slightly mixed, and thus, some of the initial population in our simulations is excited directly to the dark state.

Results and Discussion

The bright state and dark state are nearly degenerate in the Franck−Condon region. To simulate excitation to the bright state, each initial trajectory basis function (TBF) is placed on whichever of S_1 or S_2 is more strongly optically coupled to S_0 (according to the magnitude of the corresponding transition dipole moment). Using this method, 15 of the initial 20 basis functions are placed on S_1 and the remainder are placed on S_2. We assess the degree to which the bright and dark states can be unambiguously assigned by examining the ratio of the magnitudes of the $S_0 \rightarrow S_1$ and $S_0 \rightarrow S_2$ squared transition dipole moments

$$\left|\mu_{S_0 \rightarrow S_1}\right|^2 = \left|\langle \psi_{S_0} | \vec{\mu} | \psi_{S_1} \rangle\right|^2 \quad (1)$$

at the initially chosen geometries. The values of this ratio are shown in the histograms in Figure 2. With few exceptions, the assignment is unambiguous since the ratio is significantly greater than 1. In principle, if there were a significant number of cases where there was ambiguity in the assignment, one could include a pair of basis functions for each initial geometry (one on the S_1 electronic state and the other on the S_2 electronic state) and then begin the dynamics with a linear combination that maximizes the optical coupling. Alternatively (and more accurately), one could include the excitation laser pulse in the simulation, with all initial basis functions on the ground electronic state.[88]

Although the energetic ordering of the bright and dark states is variable in the Franck−Condon region, this ordering quickly becomes well-defined as the initial TBFs relax on the excited state. Figure 3 shows the squared transition dipole moment at the centroid of each initially excited TBF as a function of time for the first 10 fs after excitation. For each TBF, the S_2/S_0 and S_1/S_0 optical couplings are shown in the upper and lower panels, respectively. Within 5 fs, the lower S_1 state is unambiguously dark and the upper S_2 state is unambiguously bright. Thus, the dark state is favored by the initial relaxation.

Because the bright and dark states are reordered shortly after excitation, it is not surprising that nonadiabatic effects are observed. As can be seen in Figure 4, 55% of the population is transferred diabatically to S_2 (maintaining the character of the bright 1^1B_u state) after the initial relaxation on the excited state.

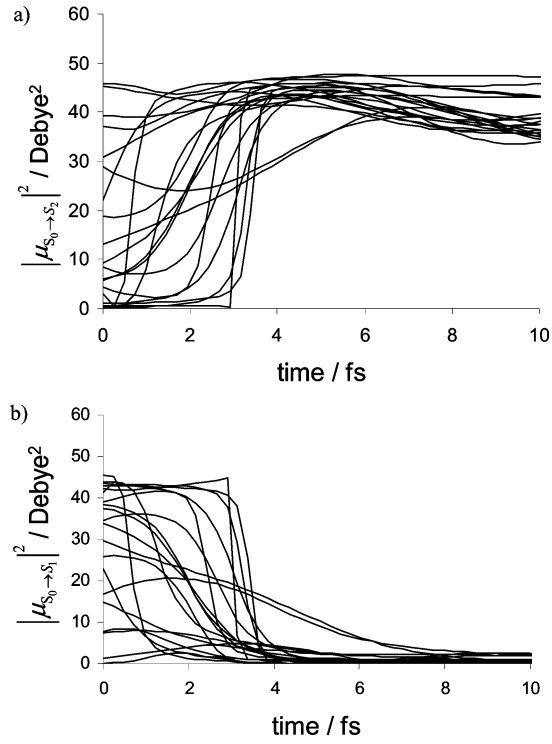

Figure 3. (a) $S_0 \rightarrow S_2$ and (b) $S_0 \rightarrow S_1$ squared transition dipole moments calculated for the first 10 fs of dynamics of each of the 20 initial TBFs. In the first few femtoseconds after excitation the bright 1^1B_u and dark 2^1A_g states mix. Within 5 fs after photoexcitation, S_1 is the dark state and S_2 is the bright state for all 20 TBFs.

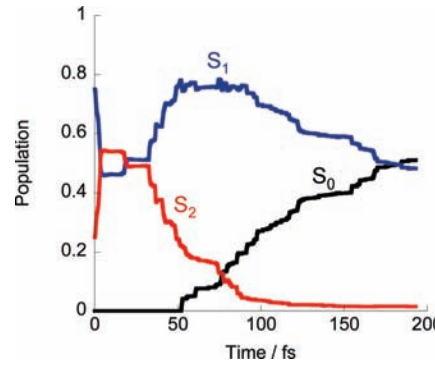

Figure 4. Population on S_2 (red), S_1 (blue), and S_0 (black) averaged over all simulations. The population starts on the brighter of the two adiabatic states, which is S_1 for 75% of the simulations. It immediately hits an intersection with the dark state, and much of the population transfers diabatically to S_2. After 20 fs the population is almost evenly split between S_1 and S_2, which in general correspond to the dark and bright states, respectively. Quenching of the population on S_2 back to S_1 begins only after significant geometric distortion on S_2. Notice that population decay to the ground state does not begin until 50 fs after excitation and is about halfway complete at 180 fs.

The remainder of the population is on S_1, which has dark 2^1A_g character after this nonadiabatic event. The 45% of the population which is found to be on the dark state may be somewhat overestimated because our approximate initial conditions place some population initially on the dark state. However, as can be seen from Figure 2, this is a small effect which will not affect even the semiquantitative conclusions made here.

Figure 5 shows the motion in the bond alternation coordinate (averaged over all simulations and both S_2 and S_1 electronic states). Bond alternation, the simultaneous lengthening and contraction of alternate carbon−carbon bonds, is an important motion in the first 50 fs after excitation. This is consistent with

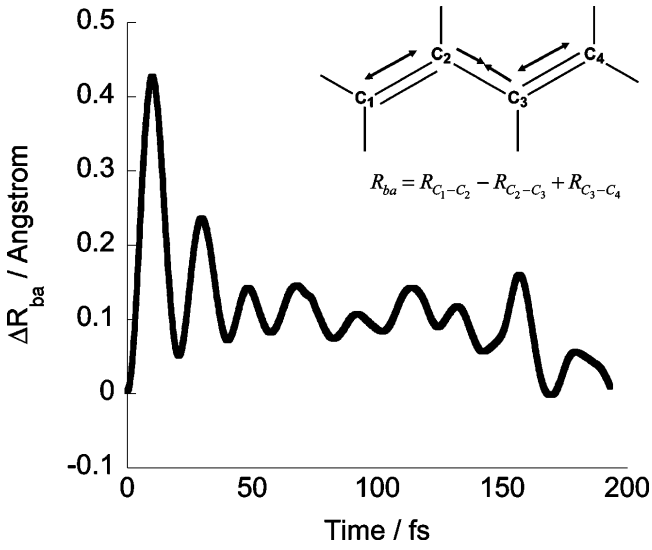

Figure 5. Deviation of the bond alternation coordinate (see the inset) from its S_0 equilibrium value (1.25 Å) averaged over all simulations and both S_2 and S_1 electronic states. The bond alternation coordinate (illustrated in the inset) is defined as the sum of the terminal carbon−carbon bond lengths minus the center carbon−carbon bond length. Motion in the bond alternation mode is very important in the first 50 fs after excitation. After 50 fs, the bond alternation coordinate relaxes toward its ground-state value.

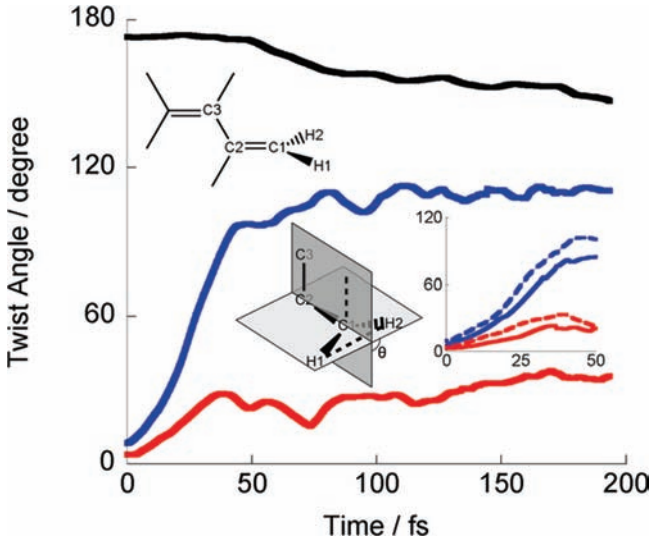

Figure 6. Expectation values of the backbone dihedral angle ($\angle C_1C_2C_3C_4$, black) and terminal C−C bond twist angles (blue and red) as a function of time after photoexcitation of butadiene (averaged over all electronic states and all initial conditions). The terminal C−C twist angles are defined as the angle (θ in the inset) between two planes (light and dark gray in the inset). The first plane (light gray) is spanned by the vector connecting H_1 and H_2 and the vector connecting C_1 and C_2. The second plane (dark gray) is spanned by the vector connecting C_1 and C_2 and the vector connecting C_2 and C_3. The blue and red lines are averages of the twist angle for the more and less twisted terminal bonds, respectively. The inset graph shows electronic state specific averages for the S_1 (dashed) and S_2 (solid) electronic states for the first 50 fs after excitation. Asymmetric twisting about a single terminal C−C bond is favored over simultaneous twisting of both terminal bonds. Eventually, the more twisted bond tends toward 90°. The less twisted bond and the central bond tend to remain nearly planar, but some twisting of each is observed. All angles have been shifted into the range of 0−180° prior to averaging.

experimental evidence; the progression in the electronic absorption spectrum of butadiene is assigned to bond alternation,[28] as is the strongest peak in the resonance Raman spectrum.[44]

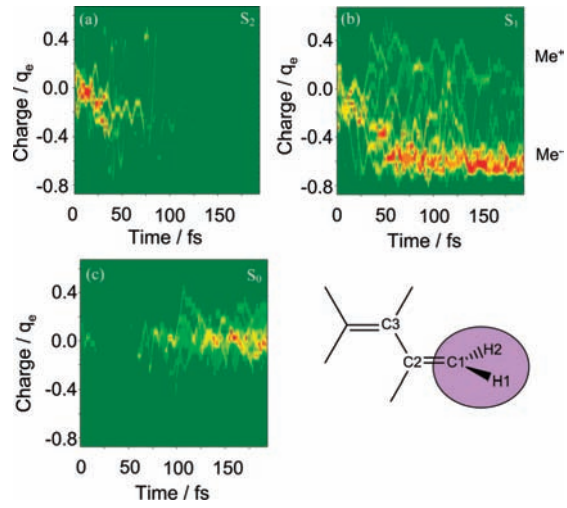

Figure 7. Time evolution of population (red is for large values and green is for vanishing values) as a function of charge on the more twisted terminal methylene unit (illustrated in the inset). The populations on S_2, S_1, and S_0 are shown in (a), (b), and (c), respectively. Charge separation initially occurs on S_2, coincident with twisting and population decay to S_1. The population on S_1 is clearly divided between two oppositely polarized charge-transfer states. These states are labeled Me^+ and Me^- according to the charge on the methylene group. The methyl anion species is favored relative to the methyl cation species.

On S_2, significant twisting about the terminal C−C bonds is observed in the first 50 fs after excitation. Figure 6 shows the twisting of the three carbon−carbon bonds as a function of time. Twisting about a single terminal C−C bond is strongly favored over concerted rotation of multiple bonds. The less twisted ethylene unit remains nearly planar, as does the central carbon−carbon bond.

It is important to note that twisting breaks the symmetry of the molecule; therefore, the adiabatic states in significantly twisted molecules contain components of both the 2^1A_g and 1^1B_u states. In the discussion below we will not refer to the electronic states of the twisted molecule by these symmetry labels, instead opting for adiabatic state labels (S_0, S_1, S_2). These labels specify the ordering of the states only, and should not be taken to indicate anything about the character of the electronic wave function.

As can be seen in Figure 5, the displacement along the bond alternation returns toward its ground-state value as this terminal C−C bond twisting occurs. This single terminal bond twisting motion also coincides with the beginning of charge transfer across the more twisted carbon−carbon bond. Figure 7a shows the time evolution of the population on S_2 (large values are red, and vanishing values are green) as a function of the charge on the more twisted terminal methylene unit (determined by Mulliken analysis of the electronic wave functions at the centers of all the TBFs). At about 30 fs, charge transfer *to* this methylene unit becomes evident, but a portion of the population exhibits charge transfer *from* the methylene unit. Coincident with this charge transfer is efficient quenching of the remaining S_2 population to S_1 via a seam of conical intersections. Most of the population has quenched to S_1 by 50 fs after excitation.

Lifetimes on the order of tens of femtoseconds have been measured in two pump−probe experiments on butadiene.[59,60] Two events occur on this time scale which may effect the observed signal: partial electronic transition to the dark state and geometric distortion of the bright populations which may change the ionization potential. Although it is difficult to make a definite assignment in the absence of direct simulation of the

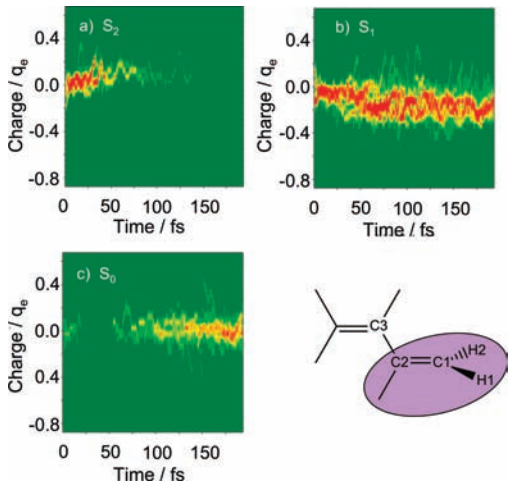

Figure 8. As in Figure 7, but for charge on the more twisted ethylene unit (illustrated in the inset). There is almost no charge separation across the central carbon−carbon bond on S_1. This reflects that the charge-transfer excitation is localized on the twisted ethylene group.

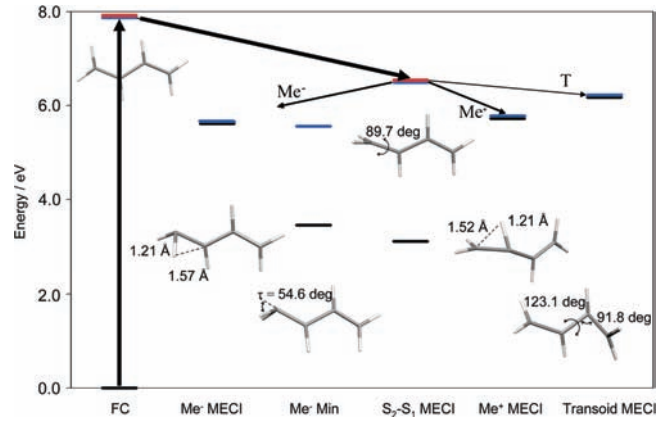

Figure 9. Points of interest along the potential energy surface optimized at the CAS(4/3) level of theory. The S_0, S_1, and S_2 energies are represented by black, blue, and red lines, respectively. Labels Me^+, Me^-, and T indicate the three MECIs on S_1. In the simulations most S_1/S_0 quenching is observed near the Me^+ and Me^- MECIs.

experimental signals, these events are certainly consistent with the observed experimental lifetimes.

Once on S_1, the molecule quickly moves into one of two "funnels" corresponding to two oppositely polarized charge-transfer states. As can be seen in Figure 7b, the population is strongly divided between a form where the more twisted methylene unit is positively charged (Me^+) and a form where it is negatively charged (Me^-). Population relaxes in both of these funnels and quenches to the ground state. In Figure 7b one can see that the Me^- funnel is favored over the Me^+ funnel.

As mentioned above, Bruckman and Salem predicted that charge transfer plays an important role in the photoisomerization of butadiene. Specifically, they predicted that the countercharge should be delocalized over the entire allyl unit as depicted in Figure 1. If this were true, the charge on the ethylenic unit containing the more twisted terminal methylene would be between one-half and two-thirds that of the more twisted methylene unit. The lower value of one-half would be expected in the case where the allyl fragment was anionic (Me^+) and the upper value of two-thirds in the case where the allyl fragment was cationic (Me^-), according to simple molecular orbital pictures. Figure 8 shows the charge on the ethylenic unit containing the more twisted terminal methylene group. Almost no charge separation can be seen on any state, including S_1 where charge separation across the twisted terminal bond is quite large. This indicates that the charge-transfer excitation is localized on the ethylenic unit containing the twisted terminal methylene and is not consistent with Salem and Bruckman's proposed methylene−allyl zwitterionic description. As can be seen in Figures 7c and 8c, there is no signature of charge transfer after quenching to S_0, as expected. The simulation time is too short to make any statements about the dynamics on the ground state, but it is possible that the Me^+ and Me^- funnels lead to different photoproducts.

To validate and analyze the PES, time-independent quantum chemistry optimizations and potential energy scans were applied. Three quantum chemical methods were employed in this work: SA3-CAS(4/3)/6-31G, SA3-CAS(4/4)/6-31G, and SA3-CAS(4/4)-MSPT2/6-31G** levels of theory. These will be abbreviated CAS(4/3), CAS(4/4), and CAS(4/4)-MSPT2, respectively. The CAS(4/4)-MSPT2 method is expected to be the most accurate of these methods and is therefore used as the target against which to judge the accuracy of the two CASSCF methods. Figure 9 shows several optimized points of interest on the CAS(4/3) PES, and Table 1 shows the energies of these geometries optimized at all three levels of theory mentioned above.

As mentioned earlier, the two low-lying valence excited states are nearly degenerate at the S_0 minimum. As seen in Table 1, both the CAS(4/3) and CAS(4/4)-MSPT2 methods reproduce this feature of the PES accurately, but CAS(4/4) predicts an S_1/S_2 energy gap of 2.3 eV at the Franck−Condon geometry. Inclusion of the fourth π orbital in the active space introduces electron correlation in an unbalanced way that favors the covalent 2^1A_g state and leads to a qualitatively incorrect PES. The root of the problem is that CASSCF describes certain kinds of electron correlation very effectively (static correlation), while it does a poor job describing dynamic electron correlation. The net result is that larger active spaces are not necessarily better, especially when the figure of merit includes global features of multiple electronic excited states. We have discussed this at length for the case of excited-state intramolecular proton transfer in previous work.[89,90] As expected for CASSCF, which does not include dynamic electron correlation, the vertical excitation energy is found to be too high at the CAS(4/3) level of theory, 7.9 eV, compared to the experimental[27] absorption maximum at 5.92 eV. However, this discrepancy is less important in describing the excited-state dynamics of butadiene compared to the relative placement of the near-degenerate S_1 and S_2 states.

As discussed above, motion along the bond alternation coordinate dominates the early excited-state dynamics of butadiene. Thus, we compare the potential energy curves for S_1 and S_2 from the two CAS methods and CAS(4/4)-MSPT2 along this coordinate in Figure 10. Agreement between CAS(4/3) and the more reliable CAS(4/4)-MSPT2 is excellent. Although the CAS(4/4) excited-state curves are correctly shaped, the gap between them is far too large.

The S_2/S_1 MECI geometry shown in Figure 9 was optimized using a representative spawning geometry selected from the dynamics simulations as the starting point. This optimized intersection geometry is an absolute minimum on the S_2 surface, which results in the efficient decay to S_1 seen in the AIMS dynamics simulations. The main feature of this geometry is that it is 90° twisted about one of the terminal carbon−carbon bonds, and otherwise essentially planar. Optimization at the CAS(4/4)-MSPT2 level of theory gives a qualitatively similar geometry. As can be seen in Table 2, the C−C bond lengths at this S_2/S_1

TABLE 1: Energies Relative to the Ground-State Minimum Energy for Geometries Optimized at Three Levels of Theory[a]

	CAS(4/3)			CAS(4/4)-MSPT2			CAS(4/4)		
	S_0	S_1	S_2	S_0	S_1	S_2	S_0	S_1	S_2
S_0 min (f_{S_0/S_n})	0.00	7.87 (1.08)	7.92 (0.0)	0.00	6.34 (0.70)	6.47 (0.0)	0.00	6.49 (0.0)	8.77 (1.02)
S_2/S_1 CI	3.12	6.49	6.55	2.61	5.81	5.83	3.03	6.31	6.31
Me^- S_1/S_0 CI	5.67	5.67	10.84	4.31	4.34	7.62	5.86	5.87	10.86
Me^- S_1 min	3.47	5.56	8.62	n/a	n/a	n/a	n/a	n/a	n/a
Me^+ S_1/S_0 CI	5.78	5.78	10.93	4.53	4.54	7.53	6.39	6.39	9.33
transoid S_1/S_0 CI	6.23	6.23	10.64	4.58	4.60	8.20	5.05	5.11	9.78

[a] There is qualitative agreement between CAS(4/3) and MSPT2, while CAS(4/4) strongly favors the transoid intersection. Oscillator strengths (f_{S_0/S_n}) for transitions from the ground electronic state at the Franck−Condon point are shown in parentheses. Despite considerable effort, we could not locate a Me^- minimum on S_1 using either CAS(4/4) or MSPT2.

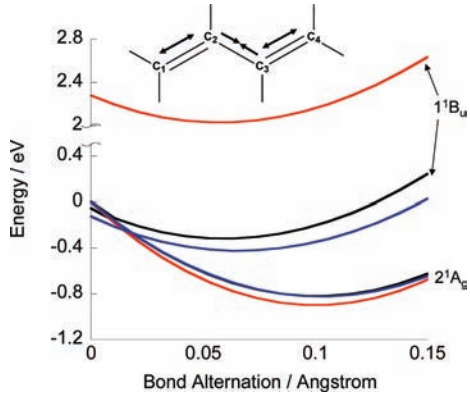

Figure 10. Potential energy curves for S_1 and S_2 along the bond alternation coordinate from the Franck−Condon point. The arrows in the inset define the bond alternation coordinate (see also Figure 5), which involves equal compression and extension of the indicated bonds. All other internal coordinates are held constant at ground-state equilibrium values. The results obtained with a CAS(4/3) wave function (black) are compared to results using CAS(4/4)-MSPT2 (blue) and CAS(4/4) (red). In all cases, the zero of energy is defined as the 2^1A_g energy at the Franck−Condon point. Agreement between CAS(4/3) and CAS(4/4)-MSPT2 is good. In contrast, the CAS(4/4) method incorrectly predicts a large gap between the two low-lying excited states.

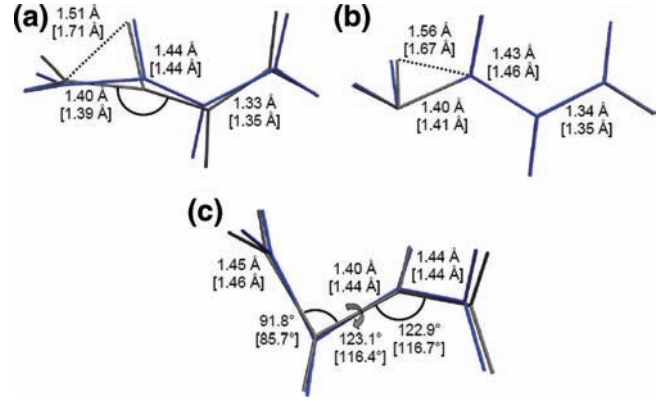

Figure 11. Geometries of the three S_1/S_0 minimal energy conical intersections: (a) Me^+ MECI, (b) Me^- MECI, and (c) transoid (T) MECI. Geometries optimized with CAS(4/3) and CAS(4/4)-MSPT2 are shown in gray and blue, respectively. Selected geometric parameters are shown with the CAS(4/4)-MSPT2 values in brackets. In all three cases the optimized CAS(4/3) and CAS(4/4)-MSPT2 geometries are qualitatively similar. The greatest difference occurs for the Me^+ intersection where CAS(4/4)-MSPT2 predicts a greater degree of hydrogen migration character than does CAS(4/3).

TABLE 2: Twisted Terminal, Central, and Untwisted Terminal Carbon−Carbon Bond Lengths for Geometries Optimized at Two Levels of Theory[a]

	CAS(4/3)			CAS(4/4)-MSPT2		
	twisted	central	untwisted	twisted	central	untwisted
S_0 min	1.35	1.47	1.35	1.35	1.46	1.35
S_2/S_1 CI	1.35	1.44	1.34	1.36	1.41	1.33
Me^+ CI	1.40	1.44	1.33	1.39	1.44	1.35
Me^- CI	1.40	1.43	1.34	1.41	1.46	1.35
Me^- min	1.41	1.42	1.35	n/a	n/a	n/a
transoid CI	1.45	1.40	1.44	1.46	1.44	1.44

[a] Notice that central and untwisted terminal bond lengths for the S_2/S_1 and charge-transfer intersections match those for the ground-state minimum.

intersection suggest that the C−C bond orders are already returning to their ground-state values when this intersection is reached.

In a study of the photoinduced ring-opening of cyclobutene, Celani et al. have previously optimized S_2/S_1 conical intersections within symmetry constraints.[11] Their choice of symmetry constraints precludes them from obtaining the MECI described above, because they allow only conrotatory or disrotatory motion (concerted rotation of the two terminal methylene groups). As seen in our dynamics simulations, rotation about only one double bond is energetically preferred when butadiene is excited. It is possible that their constrained MECIs fall on the same seam as our fully optimized MECI, and the region of the intersection seam described by their optimizations is likely relevant to photoinduced ring-opening in cyclobutene, but apparently not to the photoisomerization of *trans*-butadiene.

After quenching to S_1, population is split between two funnels corresponding to a pair of charge-transfer states where the more twisted methylene unit is either positively or negatively charged. In Figure 9, these funnels are labeled Me^+ MECI and Me^- MECI, respectively. The Me^+ MECI has significant H-migration character, as can be seen from the labeled C−H distance. The central carbon adjacent to the most twisted terminal carbon atom is pyramidalized significantly. This S_1/S_0 MECI is an absolute minimum on the S_1 surface, explaining the efficient quenching seen in the dynamics. As can be seen in Figure 11a, optimization at the CAS(4/4)-MSPT2 level of theory gives a qualitatively similar MECI geometry, although there is somewhat less H-migration character.

Searching for a minimal energy conical intersection starting from a representative spawning geometry in the Me^- funnel, we located the Me^- S_1/S_0 MECI. The Me^- MECI geometry is pyramidalized about the twisted terminal carbon and also exhibits H-migration character (but with the terminal H atom migrating compared to a central H atom in the Me^+ MECI). Unlike the Me^+ MECI, the Me^- MECI is not an absolute minimum on the S_1 PES. As seen in Figure 9, the Me^- minimum energy geometry is pyramidalized about the twisted terminal carbon, but has no H-migration character. The Me^- MECI is

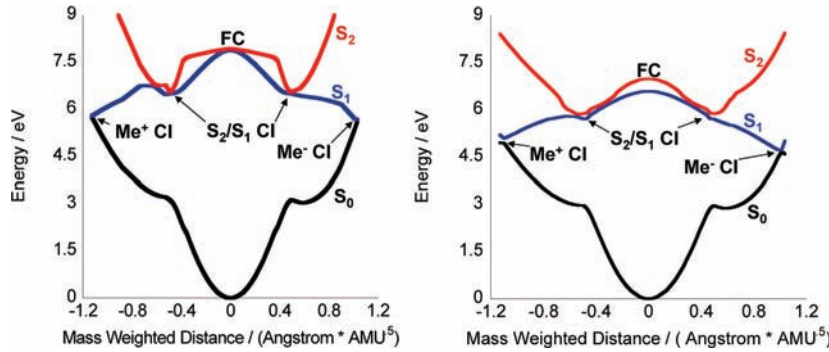

Figure 12. Potential energy surfaces along linearly interpolated (in internal coordinates) paths from the Franck−Condon point to the important MECIs calculated using CAS(4/3) (left) and SA4-CAS(4/4)*SDCI/6-31G** with Davidson correction (right). The S_0, S_1, and S_2 surfaces are shown in black, blue, and red, respectively. The Franck−Condon (FC) point is placed at 0 on the x axis. To the right the path is linearly interpolated to the S_2/S_1 MECI and then to the Me^- MECI. To the left the path is linearly interpolated to the S_2/S_1 MECI and then to the Me^+ MECI. The good agreement between the CAS(4/3) curves (used in the AIMS dynamics) and the more trustworthy MRSDCI curves argues for the validity of the AIMS simulations.

only 0.11 eV above the Me^- minimum at the CAS(4/3) level of theory, and thus, one does not expect significant trapping in this minimum. As shown in Figure 11b, optimization of this Me^- MECI at the CAS(4/4)-MSPT2 level of theory yields essentially the same geometry.

Figure 12 shows linearly interpolated paths from the Franck−Condon point to the S_2/S_1 MECI, and then from the S_2/S_1 MECI to each of the two charge-transfer S_1/S_0 MECIs. Calculations at two levels of theory are presented: CAS(4/3) and SA4-CAS(4/4)*SDCI/6-31G** with Davidson correction.[91] Agreement between the CAS(4/3) level of theory used in our dynamics simulations and the more trustworthy MRCISD calculations is quite good. After the initial nonadiabatic event a portion of the population twists about a terminal carbon−carbon bond on both S_2 and S_1. The path from the Franck−Condon region to the S_2/S_1 conical intersection seam, which basically amounts to twisting about a terminal C−C bond, is essentially barrierless on both states. Once twisted, population on S_2 quenches to S_1 and then relaxes toward one of the charge-transfer intersections. The path from the S_2/S_1 intersection to the Me^- intersection is barrierless. The linearly interpolated path from the S_2/S_1 MECI to the Me^+ MECI shows a small barrier, but this is in both cases (CAS and MRCISD) negligible compared to the energy available after Franck−Condon excitation. In any case, barrier heights along a linearly interpolated path are at best upper bounds, and the Me^+ intersection is often accessed within 200 fs in the dynamics simulations. Hence, there likely exists an alternate barrierless path.

There is a third funnel corresponding to a state of covalent character, labeled T in Figure 9. The transoid S_1/S_0 MECI, which is often discussed in the literature,[10] is an absolute minimum in this funnel. Figure 11c shows the transoid S_1/S_0 MECI geometries optimized at the CAS(4/3) and CAS(4/4)-MSPT2 levels. They are found to be in good agreement. According to the CAS(4/3) method, the transoid MECI is less than 0.5 eV above the ionic intersections, and all three of the Me^+, Me^-, and transoid MECI geometries are energetically accessible after photoexcitation. Nevertheless, we find that the transoid MECI plays a very minor role in the dynamics. Figure 13 shows all $S_1 \rightarrow S_0$ spawning geometries from the dynamics simulations divided into three groups depending on which S_1/S_0 MECI geometry they are most similar to (determined by computing the root mean squared deviation in mass-weighted coordinates). A total of 20% of the population is transferred to S_0 near geometries which best fit the Me^+ MECI, 32% near the Me^- MECI, and 5% near the transoid MECI. The remaining 43% of the population is still on S_1 at the end of our simulations.

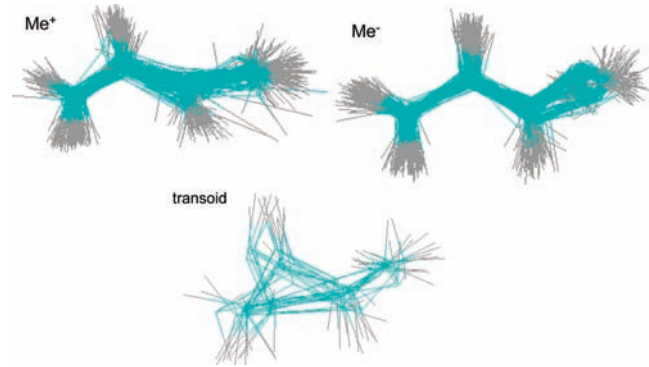

Figure 13. $S_1 \rightarrow S_0$ spawning geometries (total of 222) grouped according to similarity to the three S_1/S_0 minimal energy conical intersections. The most similar MECI is defined as the MECI to which the spawning geometry has the lowest root mean squared deviation in mass-weighted coordinates. There are 104 geometries of Me^+ character, 100 with Me^- character, and only 18 with transoid character. These spawning events result in the quenching of 20%, 32%, and 5% of the total population to the ground state, respectively. The remainder of the population remains on S_1 or S_2 at the end of the simulation.

To further analyze the relative importance of these three intersections, it is interesting to compare the relative energies of the various MECI geometries optimized at the various levels of theory, as shown in Table 1. The CAS(4/3) method puts the Me^+ and Me^- MECIs lower than the transoid MECI by 0.45 and 0.56 eV, respectively. As shown in Figure 14, optimization at the CAS(4/4)-MSPT2 level verifies that all three MECIs exist and that they are similar in energy. The MS-CASPT2 results suggest that the transoid MECI may be somewhat disfavored at the CAS(4/3) level of theory, and therefore, the covalent mechanism may be somewhat more important than suggested by our simulation. For comparison, consider the same features of the PES at the CAS(4/4) level of theory. While MSPT2 and CAS(4/3) find the three MECIs to lie within a range of 0.26 and 0.56 eV, respectively, the CAS(4/4) method finds the energetic range to be a much larger 1.28 eV. Furthermore, the CAS(4/4) method is alone in predicting that the transoid MECI is the lowest of the three S_1/S_0 MECIs. Thus, the more intuitive choice of active space produces results in qualitative disagreement with more accurate MSPT2 calculations. This again suggests that including the fourth π orbital in the active space introduces correlation effects in an unbalanced way, incorrectly favoring the covalent states. This leads to undue emphasis on

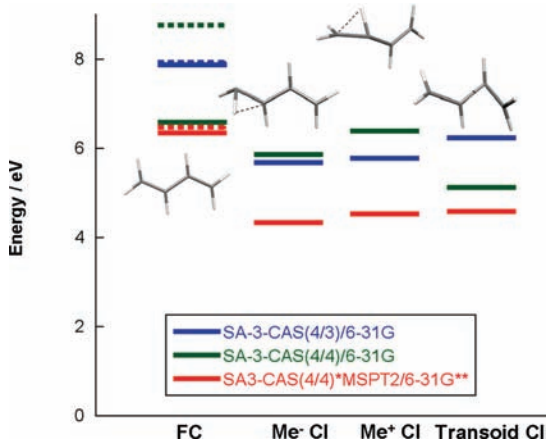

Figure 14. Relative energies at the Franck−Condon (FC) point and three important S_1/S_0 MECI geometries of butadiene at three levels of theory. The S_1 energies are shown with solid lines, while the S_2 (optically bright state) energies at the FC point are shown with dashed lines. All three intersections are energetically accessible from the FC point for all three levels of theory. CAS(4/4) strongly favors the transoid MECI relative to the charge-transfer MECIs. Although CAS(4/3) slightly disfavors the transoid intersection, it reproduces the MS-CASPT2 energetic ordering and the fact that all three MECIs are comparable in energy.

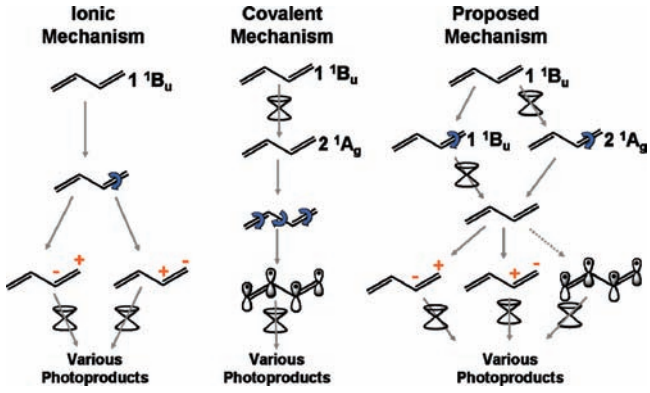

Figure 15. Schematic depiction of the two previous mechanisms (ionic and covalent) for photodynamics of *trans*-butadiene and the mechanism supported by the AIMS calculations reported in this work. Note that the proposed mechanism contains elements of both the ionic and covalent mechanisms. Dotted arrows are used to indicate minor pathways.

the role of the transoid MECI in the photochemical mechanism of *trans*-butadiene when CAS-(4/4) is used.

Conclusions

AIMS simulations of *s-trans*-butadiene were performed. In the initial 5 fs after excitation, the molecule undergoes nonadiabatic transitions which result in 55% of the excited population remaining on the bright 1^1B_u state and the remainder transferring to the dark 2^1A_g state. In contrast to longer polyenes, which transfer to the dark state without breaking planarity, butadiene twists about a single terminal carbon−carbon bond regardless of whether it is on the bright (1B) or dark (2A) state.

After twisting, the remaining S_2 population quenches to S_1 through a seam of conical intersections. The population on S_1 is split between two oppositely polarized charge-transfer states. Population in both wells quenches to the ground state quickly via conical intersections. Half of the population has quenched to the ground state (S_0) within 200 fs after the photoexcitation.

Conical intersections and energy minima have been optimized at two CASSCF levels of theory and one MS-CASPT2 level of theory, and it is found that the CAS(4/3) level of theory used in our dynamics simulations agrees considerably better with MS-CASPT2 than the more usual CAS(4/4) method. The accuracy of CAS(4/3) when compared with MS-CASPT2 validates our simulations. It also serves to point out that bigger is not always better where active spaces are concerned, nor does the "chemically intuitive" choice always yield reasonable results. The balanced treatment of correlation effects by smaller active spaces bears itself out in other polyenes as well (see the Supporting Information). Only through comparison with more reliable methods that include dynamic electron correlation can a CASSCF PES be validated.

Our dynamics simulations suggest that charge transfer plays an important role in the photodynamics of *trans*-butadiene, at variance with the currently accepted mechanism that emphasizes quenching through a covalent transoid MECI. In Figure 15, we compare the two previously proposed mechanisms (deduced using electronic structure methods which could not treat both covalent and ionic states in a balanced way) with the mechanism found in the present work. Although our new mechanism contains elements of both previously proposed mechanisms, we find the currently accepted covalent mechanism to be a minor pathway. Future dynamics simulations at the MSPT2 or MRCI levels will be able to better quantitatively assess the relative importance of ionic and covalent mechanisms, but the present work demands reconsideration of the conventional wisdom concerning the dominant role of the transoid covalent MECI.

Acknowledgment. This work was supported by the National Science Foundation (Grant CHE-07-19291). B.G.L. is a Lubrizol Fellow.

Supporting Information Available: Cartesian coordinates of all optimized structures discussed in the text and data regarding the relative energies of the 1B and 2A states of octatetraene as a function of the chosen active space. This material is available free of charge via the Internet at http://pubs.acs.org.

References and Notes

(1) Levine, B. G.; Martinez, T. J. *Annu. Rev. Phys. Chem.* **2007**, *58*, 613.
(2) Dugave, C.; Demange, L. *Chem. Rev.* **2003**, *103*, 2475.
(3) van der Horst, M.; Hellingwerf, K. *Acc. Chem. Res.* **2004**, *37*, 13.
(4) Birge, R.; Gillespie, N.; Izaguirre, E.; Kusnetzow, A.; Lawrence, A.; Singh, D.; Song, Q.; Schmidt, E.; Stuart, J.; Seetharaman, S.; Wise, K. *J. Phys. Chem.* **1999**, *103B*, 10746.
(5) Martinez, T. J. *Acc. Chem. Res.* **2006**, *39*, 119.
(6) Lumento, F.; Zanirato, V.; Fusi, S.; Busi, E.; Latterini, L.; Elisei, F.; Sinicropi, A.; Andruniow, T.; Ferre, N.; Basosi, R.; Olivucci, M. *Angew. Chem., Int. Ed.* **2006**, *46*, 414.
(7) Dou, Y.; Torralva, B. R.; Allen, R. E. *J. Phys. Chem.* **2003**, *A107*, 8817.
(8) Nonnenberg, C.; Grimm, S.; Frank, I. *J. Chem. Phys.* **2003**, *119*, 11585.
(9) Ito, M.; Ohmine, I. *J. Chem. Phys.* **1997**, *106*, 3159.
(10) Olivucci, M.; Ragazos, I. N.; Bernardi, F.; Robb, M. A. *J. Am. Chem. Soc.* **1993**, *115*, 3710.
(11) Celani, P.; Bernardi, F.; Olivucci, M.; Robb, M. A. *J. Chem. Phys.* **1995**, *102*, 5733.
(12) Strickler, S. J.; Berg, R. A. *J. Chem. Phys.* **1962**, *37*, 814.
(13) Birks, J. B.; Dyson, D. J. *Proc. R. Soc. London* **1963**, *A275*, 135.
(14) Hausser, K. W.; Kuhn, R.; Kuhn, E. *Z. Phys. Chem.* **1935**, *B29*, 147.
(15) Hudson, B. S.; Kohler, B. *Chem. Phys. Lett.* **1972**, *14*, 299.
(16) Hudson, B. S.; Kohler, B. *J. Chem. Phys.* **1973**, *59*, 4984.
(17) Hudson, B. S.; Kohler, B. E.; Schulten, K. Linear Polyene Electronic-Structure and Potential Surfaces. In *Excited States*; Lim, E. C., Ed.; Academic Press: New York, 1982; Vol. 6; p 1.
(18) Ikeyama, T.; Azumi, T. *J. Chem. Phys.* **1982**, *76*, 5672.

(19) Henneker, W. H.; Siebrand, W.; Zgierski, M. Z. *J. Chem. Phys.* **1983**, *79*, 2495.
(20) Hudson, B. S.; Kohler, B. *Annu. Rev. Phys. Chem.* **1974**, *25*, 437.
(21) Christensen, R. L.; Kohler, B. E. *Photochem. Photobiol.* **1973**, *18*, 293.
(22) Christensen, R. L.; Kohler, B. E. *J. Phys. Chem.* **1976**, *80*, 2197.
(23) D'Amico, K. L.; Manos, C.; Christensen, R. L. *J. Am. Chem. Soc.* **1980**, *102*, 1777.
(24) Schulten, K.; Karplus, M. *Chem. Phys. Lett.* **1972**, *14*, 305.
(25) Gavin, R. M. J.; Risemberg, S.; Rice, S. A. *J. Chem. Phys.* **1973**, *58*, 3160.
(26) Zerbetto, F.; Zgierski, M. Z. *J. Chem. Phys.* **1990**, *93*, 1235.
(27) Leopold, D. G.; Pendley, R. D.; Roebber, J. L.; Hemley, R. J.; Vaida, V. *J. Chem. Phys.* **1984**, *81*, 4218.
(28) Vaida, V. *Acc. Chem. Res.* **1986**, *19*, 114.
(29) Sension, R. J.; Hudson, B. S. *J. Chem. Phys.* **1988**, *90*, 1377.
(30) Quenneville, J.; Ben-Nun, M.; Martínez, T. J. *J. Photochem. Photobiol., A* **2001**, *144*, 229.
(31) Quenneville, J.; Martínez, T. J. *J. Phys. Chem.* **2003**, *107A*, 829.
(32) Ben-Nun, M.; Martinez, T. *J. Chem. Phys.* **2000**, *259*, 237.
(33) Ben-Nun, M.; Martínez, T. J. *Chem. Phys. Lett.* **1998**, *298*, 57.
(34) Ben-Nun, M.; Martinez, T. J. *Adv. Chem. Phys.* **2002**, *121*, 439.
(35) Barbatti, M.; Granucci, G.; Persico, M.; Lischka, H. *Chem. Phys. Lett.* **2004**, *401*, 276.
(36) Barbatti, M.; Ruckenbauer, M.; Lischka, H. *J. Chem. Phys.* **2005**, *122*, 174307.
(37) Ben-Nun, M.; Quenneville, J.; Martínez, T. J. *J. Phys. Chem.* **2000**, *104A*, 5161.
(38) Graham, R. L.; Freed, K. F. *J. Chem. Phys.* **1992**, *96*, 1304.
(39) Serrano-Andres, L.; Merchan, M.; Nebot-Gil, I.; Lindh, R.; Roos, B. O. *J. Chem. Phys.* **1993**, *98*, 3151.
(40) Cave, R. J.; Davidson, E. R. *Chem. Phys. Lett.* **1988**, *148*, 190.
(41) Cave, R. J.; Davidson, E. R. *J. Phys. Chem.* **1988**, *92*, 614.
(42) Serrano-Andres, L.; Roos, B. O.; Merchan, M. *Theor. Chim. Acta* **1994**, *87*, 387.
(43) Dallos, M.; Lischka, H. *Theor. Chim. Acc.* **2004**, *112*, 16.
(44) Chadwick, R. R.; Gerrity, D. P.; Hudson, B. S. *Chem. Phys. Lett.* **1985**, *115*, 24.
(45) Chadwick, R. R.; Strahan, G. D.; Zgierski, M. Z.; Hudson, B. S. *J. Chem. Phys.* **1991**, *95*, 7204.
(46) Vaida, V.; Turner, R. E.; Casey, J. L.; Colson, S. D. *Chem. Phys. Lett.* **1978**, *54*, 25.
(47) Doering, J. P.; McDiarmid, R. *J. Chem. Phys.* **1980**, *73*, 3617.
(48) Rothberg, L. J.; Gerrity, D. P.; Vaida, V. *J. Chem. Phys.* **1980**, *73*, 5508.
(49) Doering, J. P.; McDiarmid, R. *J. Chem. Phys.* **1981**, *75*, 2477.
(50) McDiarmid, R.; Doering, J. P. *Chem. Phys. Lett.* **1982**, *88*, 602.
(51) Buma, W. J.; Kohler, B. E.; Song, K. *J. Chem. Phys.* **1991**, *94*, 6367.
(52) Petek, H.; Bell, A. J.; Christensen, R. L.; Yoshihara, K. *J. Chem. Phys.* **1992**, *96*, 2412.
(53) Fuss, W.; Schikarski, T.; Schmid, W. E.; Trushin, S. A.; Hering, P.; Kompa, L. *J. Chem. Phys.* **1997**, *106*, 2205.
(54) Krawczyk, R. P.; Viel, A.; Manthe, U.; Domcke, W. *J. Chem. Phys.* **2003**, *119*, 1397.
(55) Myers, A. B.; Pranata, K. S. *J. Phys. Chem.* **1989**, *93*, 5079.
(56) Amstrup, B.; Langkilde, F. W.; Bajdor, K.; Wilbrandt, R. *J. Phys. Chem.* **1992**, *96*, 4794.
(57) Westerfield, C.; Myers, A. B. *Chem. Phys. Lett.* **1993**, *202*, 409.
(58) Trulson, M. O.; Mathies, R. A. *J. Phys. Chem.* **1990**, *94*, 5741.
(59) Assenmacher, F.; Gutmann, M.; Hohlneicher, G.; Stert, V.; Radloff, W. *Phys. Chem. Chem. Phys.* **2001**, *3*, 2981.
(60) Fuss, W.; Schmid, W. E.; Trushin, S. A. *Chem. Phys. Lett.* **2001**, *342*, 91.
(61) Warshel, A.; Karplus, M. *Chem. Phys. Lett.* **1972**, *17*, 7.
(62) Warshel, A.; Karplus, M. *J. Am. Chem. Soc.* **1972**, *94*, 5612.
(63) Krawczyk, R. P.; Malsch, K.; Hohlneicher, G.; Gillen, R. C.; Domcke, W. *Chem. Phys. Lett.* **2000**, *320*, 535.
(64) Woywod, C.; Livingood, W. C.; Frederick, J. H. *J. Chem. Phys.* **2000**, *112*, 613.
(65) Woywod, C.; Livingood, W. C.; Frederick, J. H. *J. Chem. Phys.* **2000**, *112*, 626.
(66) Woywod, C.; Livingood, W. C.; Frederick, J. H. *J. Chem. Phys.* **2001**, *114*, 1631.
(67) Woywod, C.; Livingood, W. C.; Frederick, J. H. *J. Chem. Phys.* **2001**, *114*, 1645.
(68) Granville, M. F.; Kohler, B. E.; Snow, J. B. *J. Chem. Phys.* **1981**, *75*, 3765.
(69) Bruckmann, P.; Salem, L. *J. Am. Chem. Soc.* **1976**, *98*, 5037.
(70) Ohmine, I. *J. Chem. Phys.* **1985**, *83*, 2348.
(71) Aoyagi, M.; Osamura, Y. *J. Am. Chem. Soc.* **1989**, *111*, 470.
(72) Liu, R. S. H. *Acc. Chem. Res.* **2001**, *34*, 555.
(73) Ruiz, D. S.; Cembran, A.; Garavelli, M.; Olivucci, M.; Fuss, W. *Photochem. Photobiol.* **2002**, *76*, 622.
(74) Garavelli, M.; Bernardi, F.; Olivucci, M.; Bearpark, M. J.; Klein, S.; Robb, M. A. *J. Phys. Chem.* **2001**, *105A*, 11496.
(75) Roos, B. O. *Adv. Chem. Phys.* **1987**, *69*, 399.
(76) Roos, B. O. *Acc. Chem. Res.* **1999**, *32*, 137.
(77) Finley, J.; Malmqvist, P.-A.; Roos, B. O.; Serrano-Andres, L. *Chem. Phys. Lett.* **1998**, *288*, 299.
(78) Werner, H.-J. *Mol. Phys.* **1996**, *89*, 645.
(79) Werner, H.-J.; Knowles, P. J. *J. Chem. Phys.* **1985**, *82*, 5053.
(80) Celani, P.; Werner, H.-J. *J. Chem. Phys.* **2000**, *112*, 5546.
(81) Knowles, P. J.; Werner, H.-J. *Theor. Chim. Acta* **1992**, *84*, 95.
(82) Knowles, P. J.; Werner, H.-J. *Chem. Phys. Lett.* **1985**, *115*, 259.
(83) Levine, B. G.; Coe, J. D.; Martinez, T. J. *J. Phys. Chem.* **2008**, *112B*, 405.
(84) Ben-Nun, M.; Martínez, T. J. *J. Chem. Phys.* **1998**, *108*, 7244.
(85) Levine, B. G.; Coe, J. D.; Virshup, A.; Martinez, T. *J. Chem. Phys.* **2008**, *347*, 3.
(86) Hack, M. D.; Wensmann, A. M.; Truhlar, D. G.; Ben-Nun, M.; Martínez, T. J. *J. Chem. Phys.* **2001**, *115*, 1172.
(87) *JAGUAR*, version 6.1; Schrodinger, LLC: New York, 2005.
(88) Martínez, T. J.; Ben-Nun, M.; Ashkenazi, G. *J. Chem. Phys.* **1996**, *104*, 2847.
(89) Coe, J. D.; Martinez, T. J. *Mol. Phys.* **2008**, *106*, 537.
(90) Coe, J. D.; Martinez, T. J. *J. Phys. Chem.* **2006**, *110A*, 618.
(91) Davidson, E. R. In *The World of Quantum Chemistry*; Daudel, R., Pullman, B., Eds.; Reider: Dordrecht, The Netherlands, 1974; p 17.

JP907111U